Influence of oxidic and metallic interfaces on the magnetic damping of Permalloy thin films

Verena Ney,[1] Ruslan Salikhov,[2] Kilian Lenz,[2] Olav Hellwig,[3,2] Jürgen Lindner,[2] and Andreas Ney[1,*]
[1]*Johannes Kepler University Linz, Institute for Semiconductor and Solid State Physics, Altenberger Str. 69, 4040 Linz, Austria*
[2]*Helmholtz-Zentrum Dresden-Rossendorf, Institute of Ion Beam Physics and Materials Research, Bautzner Landstr. 400, 01328 Dresden, Germany*
[3]*Institute of Physics, University of Technology Chemnitz, Reichenhainer Str. 70, 09126 Chemnitz, Germany*

(Received 11 October 2023; revised 21 November 2023; accepted 27 November 2023; published 11 December 2023)

Magnetic damping within $Ni_{80}Fe_{20}$ (Permalloy, Py) thin films is studied via temperature- and frequency-dependent ferromagnetic resonance (FMR) experiments. While the Py thickness is kept constant at 20 nm, the environment at the film interfaces was systematically varied by fabricating a set of Py thin films grown on widely used substrates and capped with common layers, which are assumed to be suitable to prevent oxidation. The resulting frequency and temperature dependence of the FMR linewidth significantly deviates from the expected Gilbert-like behavior and especially for oxidic interfaces unwanted non-Gilbert-like contributions to the magnetic damping appear, in particular, at low temperatures. In contrast, metallic capping layers avoid non-Gilbert-like contributions. In particular, Py sandwiched in between Al metallic capping and buffer layers exhibits negligible inhomogeneous FMR linewidth broadening and a very small, purely Gilbert-like contribution of $\alpha = 0.0066(2)$ down to the lowest temperature.

DOI: 10.1103/PhysRevMaterials.7.124403

I. INTRODUCTION

The understanding of magnetic damping in ferromagnetic materials is of high importance from a fundamental point of view [1] since it dictates the magnetization dynamics. It is also one of the most crucial material's parameters for various new concepts of magnetic [2,3] and magnonic [4] devices, such as, e.g., magnonic crystals with spectral filtering [5] or magnetoplasmonic crystals [6], which all rely on low magnetic damping and its tunability [7] to ultimately achieve the goals as laid out in the magnonics roadmap [8] and the roadmap of spin-wave computing [9]. For quantifying the magnetic damping, the phenomenological Gilbert damping parameter α [10] in the Landau-Lifshitz equation [11] is the central quantity although it is well-established that other, non-Gilbert-like damping mechanisms can be at work as well, see, e.g., Ref. [12]. To date, a fundamental understanding of all relevant microscopic mechanisms contributing to the magnetic relaxation is lacking, despite significant progress in elucidating a range of contributing mechanisms. From the experimental point of view, it was major progress that the technique for frequency-dependent measurements of the ferromagnetic resonance (FMR) became available over a wide frequency range. This allows for identifying different types of magnetic damping via the characteristic frequency dependence of the FMR linewidth. In particular, this concerns the so-called inhomogeneous (frequency independent) broadening, the Gilbert(-like) homogeneous broadening (linear in frequency), and non-Gilbert-like (nonlinear in frequency) contributions like two-magnon scattering processes [13]. Broadband FMR techniques were recently combined with temperature-dependent sample environments [14,15]. This enables temperature-dependent experiments to disentangle the various contributions to the magnetic damping. These can be correlated with different models for temperature-dependent mechanisms such as defect-induced mechanisms [16] as well as conductivity- and resistivitylike contributions [17]. Recently, for example, the existence of a conductivitylike Gilbert damping in epitaxial Fe [18] was proven, which was discovered long ago in Co and Ni whiskers but not till now in Fe [19,20]. Another example of disentangling different contributions to the magnetic damping by temperature-dependent broadband FMR is the different temperature dependence of interfacial and bulklike damping extracted from a thickness series of $Ni_{80}Fe_{20}$ (Permalloy, Py) thin films [15]. It was even demonstrated that different capping layers, which are usually used to prevent oxidation of the Py film, lead to slightly different magnetic damping [1]. It should be noted that Py is a very suitable ferromagnetic metal to study magnetic damping mechanisms because its fundamental magnetic properties are well understood and established. Nevertheless, the available data for α spreads over the range of $4 - 9 \times 10^{-3}$ (see a compilation of experimental results in Fig. 2 in Ref. [21] and Table I in Ref. [22] and respective references therein). As Py is a model system of a metallic ferromagnet with low magnetic damping, this suggests that a systematic study of the environment of the ferromagnetic film is required for a better understanding and control of the intrinsic magnetic damping mechanisms.

Here, we report on a systematic study of the temperature and frequency dependence of the FMR linewidth of Py as a model system, which was grown on typical substrates and capped with different types of materials suitable for

*Corresponding author: andreas.ney@jku.at

 ©2023 American Physical Society

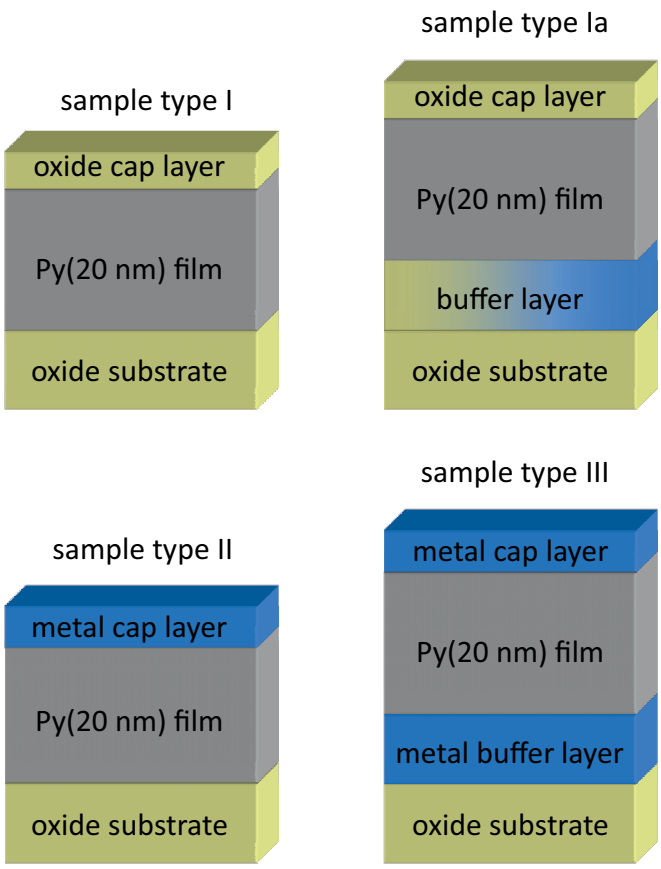

FIG. 1. Schematics of the different types of samples which were investigated throughout this paper.

preventing oxidation of the Py layer (Ta, Al, and SiO_x). To keep the number of free parameters low, the thickness of the Py layer was not varied, because the central goal of this paper is to establish the most suitable material for capping or sandwiching the Py in the sense that α shows only homogeneous, Gilbert-like contributions and is as low as possible. Surprisingly, the differences between the different substrates and capping layers exhibit a pronounced temperature dependence, which was already indicated in Ref. [15]. Nevertheless, here we can show that any interface to an oxidic material—either as cap or as substrate—leads to unfavorable contributions to the magnetic damping and a metallic sandwiching of Py in Al appears to be the best choice for further systematic studies, especially at low temperatures.

II. EXPERIMENTAL DETAILS

The Py thin films were grown by magnetron sputtering in two different preparation systems with a nominal thickness of 20 nm. The Py films were grown either on epiready *c*-plane sapphire [Al_2O_3(0001)] or on thermally oxidized Si(001) substrates. The various types of samples are sketched in Fig. 1. All capping layers have a nominal thickness of 5 nm while the buffer layers were 2 nm thick. The Py films with the SiO_x cap (sample type I) and the Ta-capped or buffered films (sample type II or III) were deposited at room temperature in a BESTEC sputter system with a base pressure of 3.5×10^{-9} mbar. Twenty standard cubic centimeters per minute (sccm) Ar flow was used as process gas. The working pressure during deposition was 3×10^{-3} mbar for Py and SiO_x, and 5×10^{-3} mbar for Ta. The dc sputter power was set to 50 W for Py and Ta, while SiO_x was deposited using rf power of 100 W. The growth rates were 0.25 nm/s, 0.068 nm/s and 0.028 nm/s for Py, Ta, and SiO_x, respectively. In addition, the SiO_x-capped films were also grown with either SiO_x or Ta buffer layers (sample type Ia). The Al-capped and buffered Py films (sample type II or III) were exclusively grown on sapphire substrates in an ultrahigh vacuum system with a base pressure of 2×10^{-9} mbar at room temperature. The working pressure was 4×10^{-3} mbar for both Al and Py using 10 sccm Ar and a sputter power of 20 W, respectively. The growth rates of 0.9 nm/s for Py and Al were monitored using a quartz crystal microbalance.

Broadband FMR measurements have been carried out using the CRYO-FMR40 setup from NANOSC with a microwave frequency f_{MW} in the range of $2 - 40$ GHz. The sample is placed on a coplanar waveguide and the transmitted power is detected by a diode. A pair of Helmholtz-coils supplies an external alternating magnetic field for lock-in detection. The static external magnetic field H_{ext} up to 9 T as well as the temperature control in the range of $4 - 295$ K is provided by a QUANTUMDESIGN PPMS system, which is controlled by the NANOSC software allowing for a fully automated recording of the FMR spectra over a wide range of temperatures and microwave frequencies. As the modulation coils create some waste heat at maximum modulation, which is required here, the lowest achievable temperature is typically 6 K. The temperature is measured directly underneath the sample/waveguide assembly. Nevertheless, in most cases, 10 K was chosen as the lowest temperature, where the cooling power of the system can easily compensate the heating from the modulation coils. The individual FMR spectra are automatically fitted with a Lorentzian, which allows to extract the relevant magnetic parameters, i.e., the resonance field H_{res} as well as the FMR linewidth ΔH. Note that throughout this work, ΔH refers to the full width at half maximum, which can be converted to the peak-to-peak linewidth ΔH_{pp} using $\Delta H = \sqrt{3} \times \Delta H_{pp}$. All samples were measured in in-plane geometry, i.e., applying H_{ext} in the plane of the film using a dedicated waveguide assembly. For a few samples, the out-of-plane geometry was also measured, which requires another dedicated waveguide assembly. Note that intermediate angles cannot be measured with this setup.

In a typical FMR experiment using the Cryo-FMR, the so-called Kittel-plots, i.e., f_{MW} as a function of $\mu_0 H_{res}$, are recorded at selected temperatures. This data can be fitted with the following equation:

$$f_{MW} = \frac{\gamma \mu_0}{2\pi} \sqrt{(M_{eff} + H_k + H_{res})(H_k + H_{res})}. \quad (1)$$

Here γ is the gyromagnetic ratio, which is related to the g factor via $\gamma = g\frac{\mu_B}{\hbar}$, where μ_B is the Bohr magneton and $\hbar$ is the reduced Planck's constant. H_{res} denotes the resonance field extracted from the individual FMR spectra, H_k is an effective in-plane anisotropy, and M_{eff} is the effective magnetization, which contains the shape anisotropy as well as an effective uniaxial out-of-plane anisotropy. Note that Eq. (1)

is only valid when the in-plane easy axis of the sample is oriented parallel to H_{ext}. In the ideal case of Py where no crystalline anisotropy should be present, H_k should be zero and M_{eff} should be equal to the shape anisotropy and, thus, the spontaneous magnetization M_s. If M_{eff} deviates from the shape anisotropy, it would indicate an additional effective uniaxial out-of-plane anisotropy. Since the Cryo-FMR only uses two fixed geometries, the full angular dependence of H_{res} could not be measured. So, it is not possible to reliably extract anisotropy parameters such as H_k. In addition, it has been noted that a slight uncertainty of the actual H_{ext} behaves similar to the effective anisotropy H_k [23]. In the PPMS system, where the actual field of the magnet is not directly measured, residual pinned flux in the superconducting magnet can easily create small offset fields typically leading to a small negative H_k of the order of 0.5 mT to 1.5 mT as discussed before [24]. For the purposes of this paper, where relative changes of the magnetic parameters as a function of temperature are the main objective, a precise determination of M_{eff}, H_k, and the g factor is deemed not to be essential. Therefore, all three parameters are fitted together as implemented in the software and mostly relative changes as a function of temperature and/or between two similar samples will be discussed. The joint fitting of all three parameters implies that their respective uncertainties are correlated, especially regarding their actual numerical values; only relative changes, e.g., as a function of temperature of the same sample can be compared within the visible scattering of the data. For the purposes of the present paper, where the magnetic damping parameters are the focus, it is sufficient to note the following accuracies: (i) absolute values for the g factor are never better than ± 0.005, (ii) all values of H_k below $1 - 1.5$ mT are insignificant and can be disregarded, and (iii) M_{eff} should be compared to the characteristic functional $M(T)$ behavior of Py; deviations from that behavior can only be taken as indicative of an additional out-of plane uniaxial anisotropy.

A second set of data can be derived from the frequency dependence of the FMR linewidth ΔH. This data can be fitted using the following equation:

$$\Delta H = \Delta H_0 + \frac{4\pi\alpha}{\gamma} f. \tag{2}$$

Here ΔH_0 is the inhomogeneous line broadening, which is frequency independent and α is the Gilbert damping parameter, which accounts for a linear frequency dependence. Deviations from the linear behavior of $\Delta H(f_{MW})$ indicate additional contributions to the FMR linewidth such as two-magnon processes which typically exhibit a nonlinear frequency dependence at lower frequencies, which becomes constant at higher f_{MW} [13] or even decreases [16]. Throughout this paper, the indicated uncertainties of the derivation of the damping parameters rely on linear regression of the data and the associated uncertainties.

III. EXPERIMENTAL RESULTS

A. Oxidic capping layers

Figure 2(a) shows the frequency-resonance field dependencies (Kittel plots) of a 20-nm-thick Py film on sapphire with a 5-nm SiO_x capping layer (sample type I) recorded

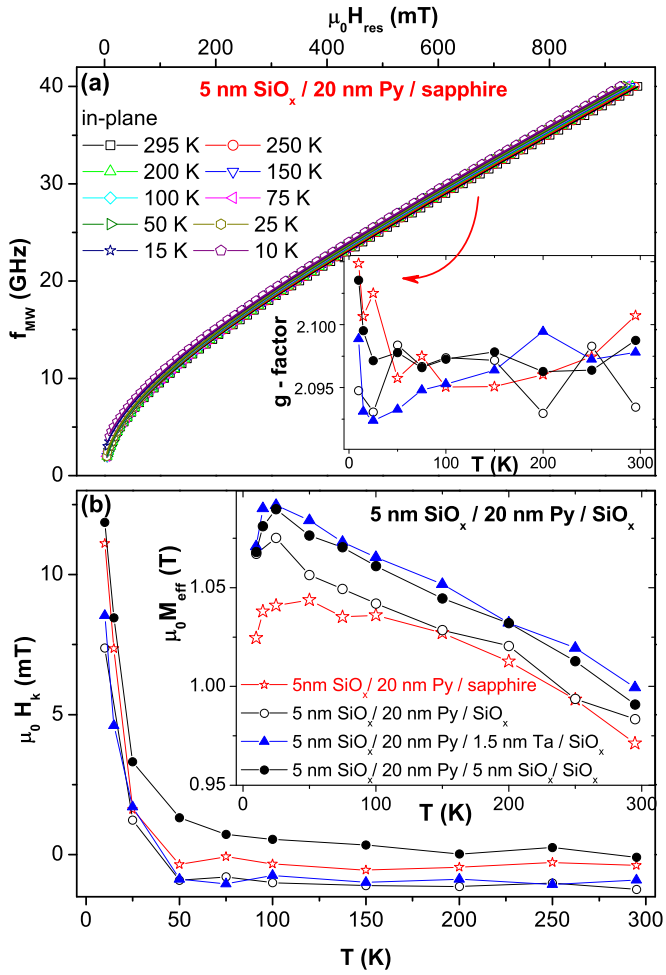

FIG. 2. (a) Kittel plot (f-H dependence) of the SiO_x-capped Py grown on sapphire measured at various temperatures in in-plane geometry. The inset shows the fitted g factor for this sample (red stars) in comparison to samples grown on Si substrates. (b) Effective in-plane anisotropy field H_k and M_{eff} (inset) as a function of temperature derived from the Kittel plots shown in (a).

between 2 and 40 GHz from 295 K down to 10 K. It reveals no very pronounced temperature-dependent effects. The inset shows the temperature dependence of the g factor, which was extracted from a fit of the data according to Eq. (1). In addition to the Py film on sapphire (open red stars), all studied samples with a SiO_x cap on silicon substrates are shown, which were grown without buffer (sample type I; open black circle), with Ta (full blue triangles) or SiO_x (full black ciurcles) buffer layers (sample type Ia). Overall, the temperature dependence of the g factor is rather weak and remains within the visible scatter of the data at different temperatures and from sample to sample. Virtually all data remains in the range of $g = 2.096(5)$ but a slight tendency for increased g factors towards low temperature is visible. This is better seen if each sample is being individually looked at but nonetheless remains within the visible scatter of the data. Figure 2(b) compiles the remaining fitted parameters for the identical set of samples, namely, the effective in-plane anisotropy field H_k and M_{eff} (inset). Down to 50 K, the values for H_k are small and mostly negative, which may be disregarded within

the achievable accuracy of the fixed-geometry measurement. However, below 50 K a significant increase of H_k up to around 10 mT is visible, which is of comparable size regardless of the substrate. Since also thin buffer layers of either Ta or SiO_x do not change this behavior, this increase has to stem from the SiO_x capping of the Py film. Likewise, the $M_{eff}(T)$ shown in the inset of Fig. 2(b) is virtually identical with the exception of the sample grown on sapphire. While the latter one exhibits a shape, which resembles typical $M(T)$ curves of Py films recorded by conventional static magnetometry, all other samples exhibit a more linear temperature dependence at low temperatures, which may be explained by an additional out-of-plane effective anisotropy, which appears in parallel to the increase of H_k. Only at the lowest temperatures is a small downturn in M_{eff} visible for all samples.

In summary, the results from the Kittel fits of the SiO_x-capped Py films are as follows: (i) The effective in-plane anisotropy field H_k exhibits a pronounced increase at low temperatures, which is (ii) also accompanied by a contribution of an effective out-of-plane anisotropy as seen from the unusual behavior of M_{eff} at low temperatures. (iii) The g factor remains temperature independent with a small tendency to slightly increase at low temperatures. Since this behavior is present in all samples with the SiO_x cap—irrespective of the type of substrate or buffer layer separating the Py from the silicon substrate—we assign this behavior to the presence of the SiO_x cap. This obviously must be induced by a slight oxidation of the Py film during growth of the SiO_x cap. It is noteworthy that the influence of the oxide capping layer is only visible at low temperatures, whereas from 100 K to ambient conditions the overall behavior appears to be inconspicuously for Py. It is therefore of special interest how these small changes due to the oxidic cap at low temperatures influence the magnetic damping.

Figure 3(a) shows the frequency dependence of the FMR linewidth ΔH of the Py film on sapphire for various temperatures. Between 295 K and 75 K, the $\Delta H(f_{MW})$ exhibits a linear behavior, which is indicative of a Gilbert-like behavior with small variations in the slope depending on temperature. At low temperatures, deviations from the linear behavior appear, and both the slope as well as the $y-$axis intercept are significantly altered. This behavior is also seen for SiO_x-capped Py grown on silicon substrates; see Fig. 5(a). This nonlinear behavior can be tentatively assigned to two-magnon processes similar to previous reports for Py/NiO [25]. Their influence can be seen in Fig. 3(b), where the results of a linear fit according to Eq. (2) are shown for the sample grown on sapphire (open red stars) as well as all SiO_x-capped films grown on silicon. In addition, SiO_x-capped Py samples with Ta or SiO_x buffer (type Ia) have been investigated since a Ta buffer has been reported to suppress two-magnon contributions in Py/NiO [25]. For all studied samples in Fig. 3(b), the inhomogeneous broadening ΔH_0 increases at low temperatures, resembling the increase of H_k seen in Fig. 2(b) for all samples with the SiO_x cap, irrespective of the substrate or buffer layer. The corresponding temperature dependence of the Gilbert damping parameter $\alpha(T)$ of all SiO_x-capped samples is shown in the inset of Fig. 3(b). Again, all samples exhibit a rather similar behavior revealing a nonmonotonous behavior with a maximum around 50 K. Such a behavior of

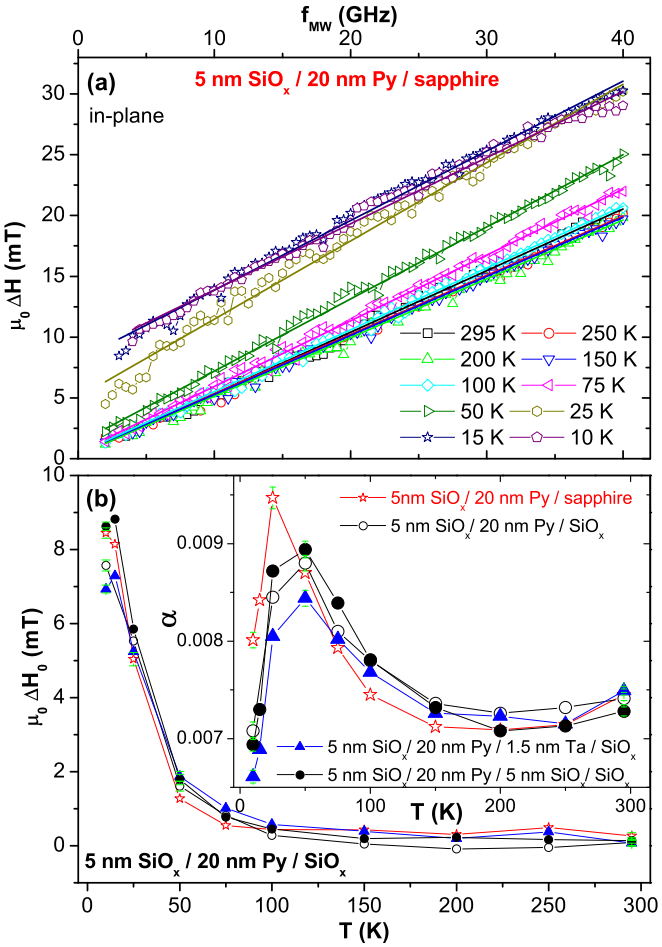

FIG. 3. (a) Frequency-dependent FMR linewidth ΔH measured with in-plane field as a function of temperature for the identical samples as in Fig. 2(a), including linear fits. Deviations are visible at lower temperatures (see text). (b) Inhomogeneous broadening ΔH_0 and homogeneous Gilbert-like damping α (inset) derived from the linear fit of the data in (a) for the identical set of samples as in Fig. 2. Error bars derived from the linear regression of the data are indicated in green for selected temperatures.

$\alpha(T)$ has been reported before for Py films grown on SiO_x-buffered silicon and capped with either TaN or Al_2O_3 [15]. In Ref. [15], this was tentatively assigned to a spin reorientation transition. However, the microwave frequency range was limited to 14 GHz. Looking at the $\Delta H(f_{MW})$ behavior in Fig. 3(a), one recognizes that deviations from the linear behavior are only visible when a wider frequency range is studied.

It has been suggested to exclude the nonlinear contributions from two-magnon scattering processes to the linewidth by fitting data only in the range of 25 to 40 GHz [24]. However, a safe elimination of such two-magnon processes to the FMR linewidth is achieved by using the out-of-plane geometry, where those effects are known to be suppressed [13]. Figure 4(a) shows the FMR linewidth ΔH as a function of the microwave frequency f_{MW} of the identical sample as in Fig. 3(a), measured in out-of-plane geometry for various temperatures. In contrast to the in-plane measurement, no deviations from the linear behavior are visible at any

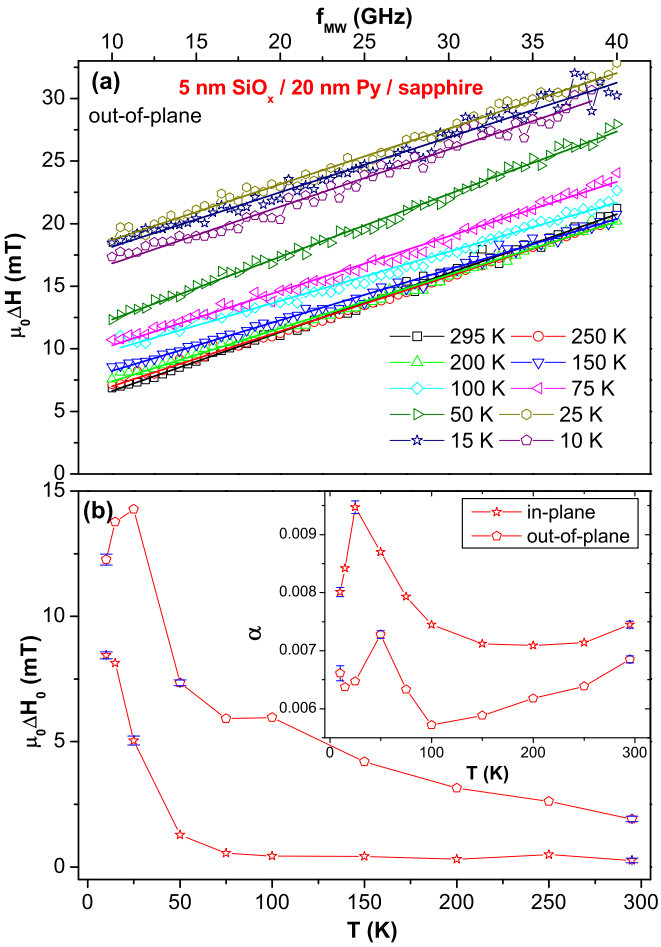

FIG. 4. (a) Frequency-dependent FMR linewidth ΔH measured with field out-of-plane as a function of temperature for the identical sample as in Figs. 2(a) and 3(a), including linear fits. (b) Inhomogeneous broadening ΔH_0 and homogeneous Gilbert-like damping α (inset) derived from the linear fit of the out-of-plane data in (a) in comparison to the in-plane data (asterisks) shown in Fig. 3(b). Error bars derived from the linear regression of the data are indicated in blue for selected temperatures.

temperature, proving that the observed kink in the in-plane data indeed stems from two-magnon scattering processes. Nonetheless, there is a pronounced temperature dependence of the FMR linewidth. Figure 4(b) compares the results of the linear fit for the out-of-plane data with the in-plane results already shown in Fig. 3(b). It is visible that the inhomogeneous broadening ΔH_0 is systematically higher in out-of-plane geometry and it steadily increases over the entire temperature range, which could be an effect of a slight misalignment of the sample due to the fixed geometry of the waveguide assembly in the Cryo-FMR. In contrast, the homogeneous, Gilbert-like damping constant α is systematically lower by about 0.001 over the entire temperature range, which can be taken as the uncertainty of the numerical value of the homogeneous α for the in-plane geometry due to two-magnon processes. Also, the nonmonotonous behavior in $\alpha(T)$ is suppressed. Only around 50 K, where M_{eff} and H_{k} in the in-plane geometry starts to deviate, $\alpha(T)$ shows a slight anomaly in the out-of-plane geometry. Looking at the $\Delta H(f_{\text{MW}})$ data in Fig. 4(a) again,

TABLE I. Compilation of the most important quantitative results of homogeneous and inhomogeneous magnetic damping for Py films with oxidic cap for selected temperatures as displayed in Figs. 3 and 4. $\Delta H_0^{300\text{ K}}$ is between 0.1 and 0.2 mT for all in-plane (IP) measurements, while for the out-of-plane (OOP) measurement it is 1.9 mT; see Fig. 4. The experimental error bars for α are in the range of ± 0.00004 and ± 0.0001.

	$\alpha^{300\text{ K}}$	$\alpha^{50\text{ K}}$	$\alpha^{10\text{ K}}$	$\Delta H_0^{10\text{ K}}$
SiO_x/Py/sapphire (IP)	0.00745	0.0087	0.00801	8.4 mT
SiO_x/Py/sapphire (OOP)	0.00685	0.00728	0.00661	12.3 mT
SiO_x/Py/SiO_x	0.00741	0.0088	0.00708	7.6 mT
SiO_x/Py/SiO_x/SiO_x	0.00728	0.00894	0.00694	8.6 mT
SiO_x/Py/Ta/SiO_x	0.00749	0.00844	0.00661	6.9 mT

one recognizes around 50 K that there is an apparent transition from a regime with a generally lower linewidth to a clearly increased FMR linewidth. However, for the purposes of the present paper, it is preferred to suppress any non-Gilbert-like contributions to the FMR linewidth rather than to investigate different unwanted contributions to it. The high inhomogeneous broadening exists in all geometries—especially at low temperatures—irrespective of the presence or absence of two-magnon scattering processes.

Summarizing this part, the use of oxidic capping layers induces changes in the effective anisotropy only at low temperatures. They have a strong influence on the magnetic damping by inducing additional damping mechanisms, leading to a nonlinear $\Delta H(f_{\text{MW}})$ behavior and an apparent nonmonotonic $\alpha(T)$ behavior with a peak around 50 K—if the nonlinear two-magnon scattering processes are disregarded. Comparing the SiO_x-capped samples grown on either sapphire or silicon with or without Ta or SiO_x buffer layers, no significant changes are found in virtually all magnetic parameters extracted from the temperature-dependent broadband FMR measurements. In particular, the magnetic damping parameters are rather similar for all studied samples except the measurement in out-of-plane geometry; see Table I. This indicates the dominant role of the oxidic cap in inducing the (unwanted) nonlinear $\Delta H(f_{\text{MW}})$ behavior due to the presence of two-magnon processes. The presence of two magnon processes requires some kind of magnetic roughness [13] whose microscopic origin cannot be unambiguously identified. It is known that Py only forms a less than 1-nm-thick oxide layer at ambient temperatures containing antiferromagnetic NiO and FeO [26]. It was attempted to confirm the presence of these oxides in the SiO_x-capped samples via exchange bias. However, after field cooling in ± 5 T down to 2 K, no horizontal shift of the $M(H)$ curve and no increase of the coercive field compared to zero-field cooling could be observed (not shown). However, this can still be consistent with the formation of only a very thin oxide layer, which can create a modified anisotropy as reported in Ref. [26], thus accounting for the strong increase in H_{k} in Fig. 2(b). In addition, an uncapped Py film was investigated and it exhibits a qualitatively very similar magnetic behavior as the SiO_x capped films (not shown), presumably due to the formation of a less well-defined oxide layer. Thus, one may consider it

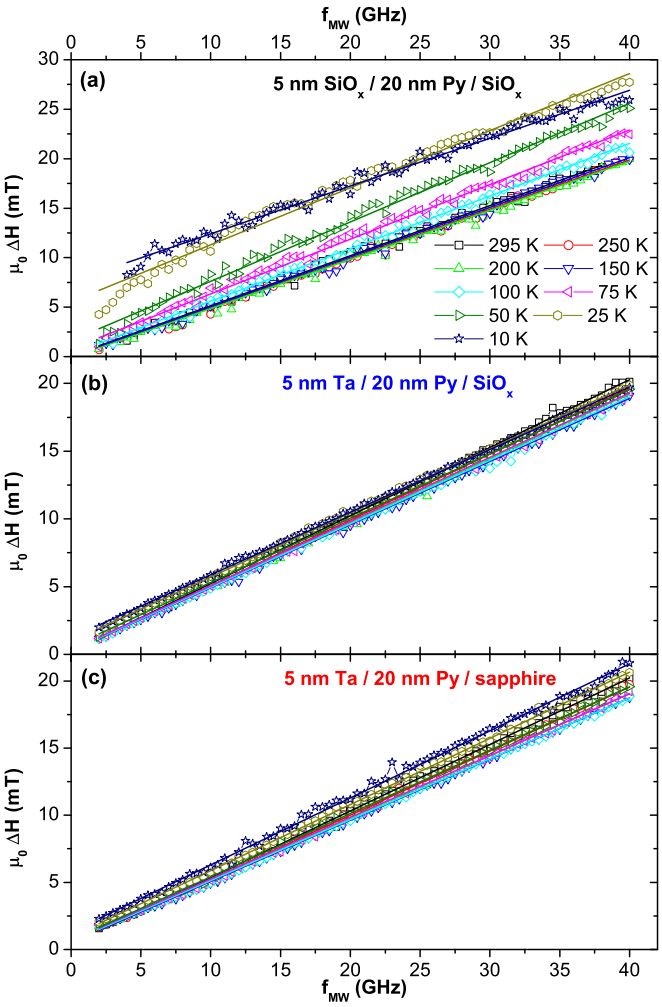

FIG. 5. (a) Frequency-dependent linewidth $\Delta H(f_{\mathrm{MW}})$ of the SiO_x-capped Py film shown in Figs. 2 and 3 as a function of temperature, revealing deviations from the linear behavior. The comparison of $\Delta H(f_{\mathrm{MW}})$ of a Ta-capped Py film grown on (b) Si with (c) sapphire substrates reveals a linear behavior.

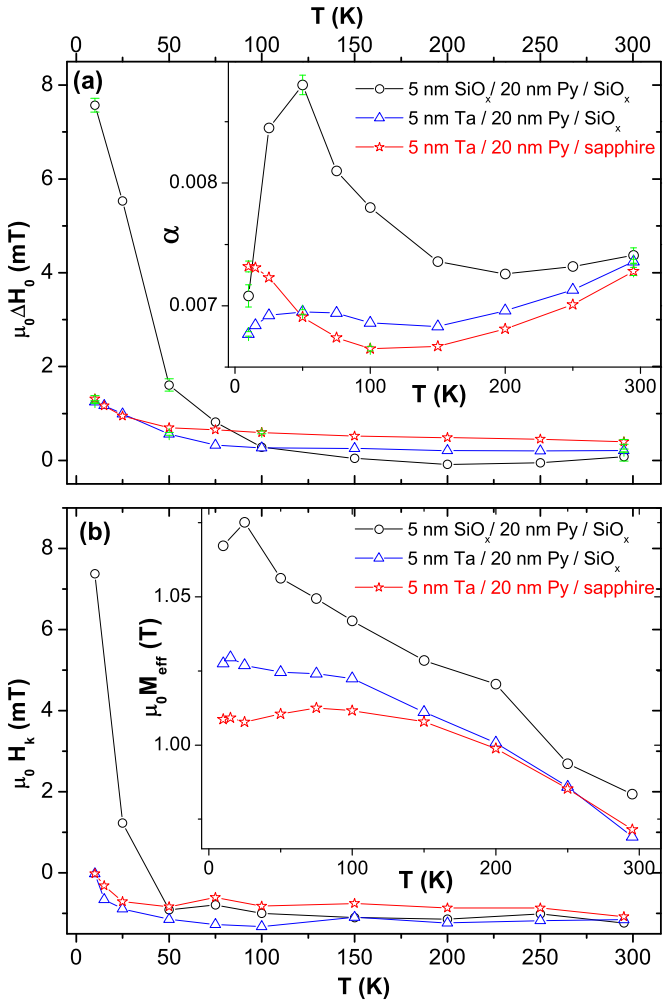

FIG. 6. (a) Resulting inhomogeneous broadening ΔH_0 and Gilbert-damping parameter α (inset) as a function of temperature of the data shown in Fig. 5. Error bars derived from the linear regression of the data are indicated in green for selected temperatures. (b) Temperature dependence of H_{k} and M_{eff} (inset) extracted from the Kittel plots of the identical set of samples.

as the most likely scenario that the two magnon processes are activated by defect formation due to slight oxidation at the interface between the oxidic cap and the Py film underneath. Therefore, in a next step, to avoid the unwanted two-magnon processes, nonoxidic capping layers shall be investigated.

B. Metallic capping layers

Figure 5 compiles the $\Delta H(f_{\mathrm{MW}})$ behavior of the Ta-capped Py films grown on silicon (b) and sapphire (c) substrates (sample type II) in comparison to the SiO_x-capped sample (type I) grown on silicon (a). As already discussed above, the latter exhibits a nonlinear $\Delta H(f_{\mathrm{MW}})$ behavior at low temperatures similar to the SiO_x-capped sample grown on sapphire in Fig. 3(a). In contrast, for the Ta-capped samples, the $\Delta H(f_{\mathrm{MW}})$ behavior is found to be linear across the entire temperature range. Obviously, the hypothesis that the SiO_x cap induces the nonlinear behavior is correct and metallic capping at first sight avoids unwanted contributions to the FMR linewidth. In addition, the second Py/oxide interface, namely, the one to the substrate does not induce non-Gilbert-like damping processes. These conclusions can be refined by looking at the extracted inhomogeneous broadening and Gilbert damping parameter in Fig. 6(a). The low-temperature increase of ΔH_0 of the oxidic cap (open black circles) is absent for Ta-capped Py films grown on either silicon (open blue triangles) or sapphire (open red stars). Likewise, the peak in the $\alpha(T)$ behavior of the oxidic cap shown in the inset of Fig. 6(a) is strongly suppressed for the Ta-capped Py grown on silicon and turns into a minimum for sapphire substrates. This underlines that the peak in $\alpha(T)$ around 50 K is not an intrinsic but an extrinsic property of Py films and is induced by interfacial effects.

The changes of the magnetic damping in this set of samples is also accompanied by respective changes in H_{k} and M_{eff}. Figure 6(b) summarizes both parameters extracted from Kittel fits for the identical set of samples as in (a). Similar to the ΔH_0, also the low-temperature increase of H_{k} induced by oxidic caps is strongly reduced in the Ta-capped films.

Likewise, also the low temperature behavior of M_{eff} changes and resembles the more usual $M(T)$ behavior of a ferromagnet. This again underlines that the oxidic cap induces effective in- and out-of-plane anisotropies at the same time, which result in an increased inhomogeneous broadening. Obviously, the Ta cap can reduce unwanted effects on the magnetic damping at low temperatures but, as Fig. 6 reveals, there seems to be a difference between sapphire and silicon substrates regarding the $\alpha(T)$ behavior as well as $M_{\mathrm{eff}}(T)$. This is a first indication, that the second oxidic interface to the substrate also influences the magnetic properties of Py. In a final step, the influence of different buffer layers will also be investigated.

C. Metallic buffer layers

Figure 7 compiles the $\Delta H(f_{\mathrm{MW}})$ behavior of three different samples (type II and III) grown on sapphire substrates. In Fig. 7(a), a Ta-capped film with Ta buffer is shown. This data can be compared with those without Ta buffer in Fig. 5(c). In addition, Fig. 7 shows an Al-capped Py film without (b) and with an Al buffer (c). At first sight, no marked differences are visible for these samples and it is obvious that the $\Delta H(f_{\mathrm{MW}})$ behavior is linear, i.e., Gilbert-like for all samples. This rules out contributions from processes like two-magnon scattering for all samples but still may include other effects like eddy current damping and/or spin pumping because of the adjacent metals. It should be noted that both capping and buffer layer were chosen to be as thin as possible to minimize these effects. A more detailed study goes beyond the scope of the present paper and will be published elsewhere. For the purposes of this paper, it is sufficient to note that both Al as well as Ta typically form a native oxide of ~3 nm thickness [27]. Therefore, the Py film is symmetrically sandwiched in a ~2 nm metallic cap and buffer, which are in contact with a natural oxide and an oxidic substrate, respectively. Even if some intermixing of the Py with the Ta/Al should occur, this should be limited to ~1 nm on either side and, thus, not more than 10% of the entire 20-nm-thick Py film. It was also verified that the thickness of the cap is sufficient to protect the Py from degradation due to oxidation. In the case of Al, this was verified by comparing nominally identical, freshly grown films with up to 3-year-old samples (not shown). For selected samples in this paper, this was verified by remeasuring the identical sample after several months of exposure to ambient conditions.

Turning back to the influence of a metallic buffer on the magnetic damping of Py films, Fig. 8 shows the extracted parameters from Kittel-fits for six different samples: open blue circles denote the Ta-capped Py on SiO_x from Fig. 5(b), open blue triangles denote the Ta-capped film on sapphire from Fig. 5(c), and open green stars Al-capped Py on sapphire from Fig. 7(b), i.e., sample type II. The respective full symbols refer to the same sample with the respective buffer layer, e.g., full triangles or stars refer to the Ta- or Al-sandwiched films (sample type III) depicted in Figs. 7(a) and 7(c), respectively. In Fig. 8(a), $M_{\mathrm{eff}}(T)$ is shown, which reveals that all buffered samples have a nearly identical M_{eff}. The value is systematically higher than for all unbuffered ones. While it cannot be decided whether this is due to a reduction in

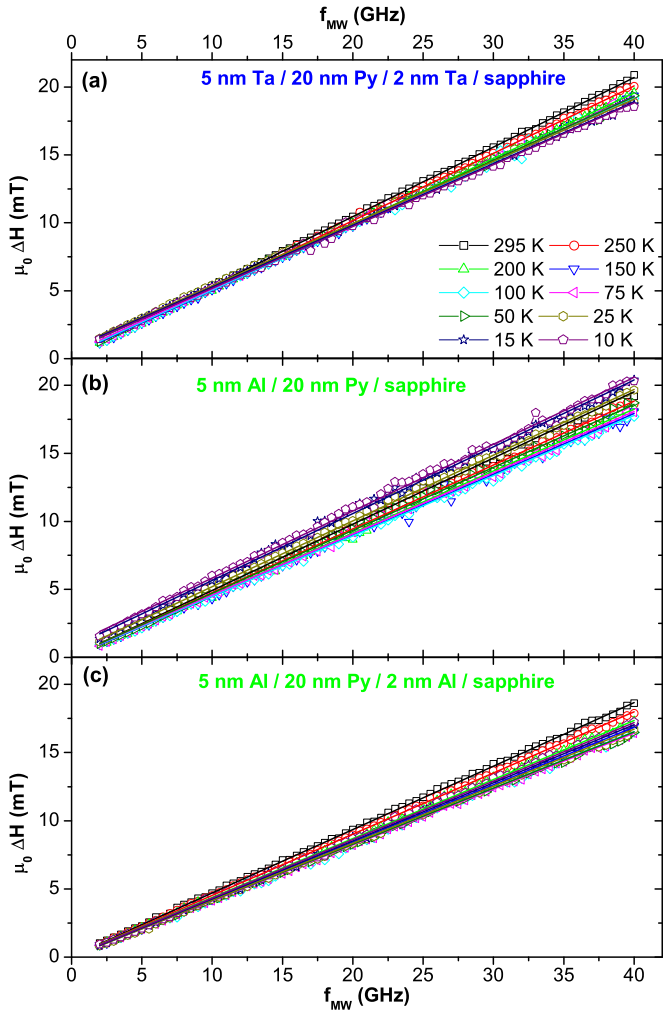

FIG. 7. Comparison between the $\Delta H(f_{\mathrm{MW}})$ of the Py film grown on sapphire with (a) Ta cap and Ta buffer, (b) Al cap only, and (c) Al cap and Al buffer recorded as a function of temperature, respectively.

M or an effective out-of-plane anisotropy, it is evident that there are discrepancies for the different substrates. For an interface with sapphire substrate (open triangles/stars), there is a small reduction in M_{eff} at low temperatures, which is absent for the silicon substrate (open circles). Likewise, the Ta cap appears to significantly reduce M_{eff} while for an Al cap M_{eff} it is systematically higher. We tentatively ascribe this to some finite amount of intermixing, which is known for the Ta/Py interface [28–30]. On the other hand, the Ta buffer appears to have no influence on M_{eff} compared to Al (see the full symbols). This may be understood by considering the (strongly kinetic) sputtering process: For the Ta cap, rather heavy Ta ions impinge on the lighter elements Ni and Fe whereas for Al the lighter ions impinge on the relatively heavier Ni and Fe atoms in the film, which may explain a relatively stronger intermixing for a Ta cap in comparison to an Al cap. In turn, for an Al buffer, the intermixing with the Py on top should be stronger compared to a Ta buffer based on the same reversed argument. Nevertheless, no systematic differences between the Al and Ta buffer can be seen.

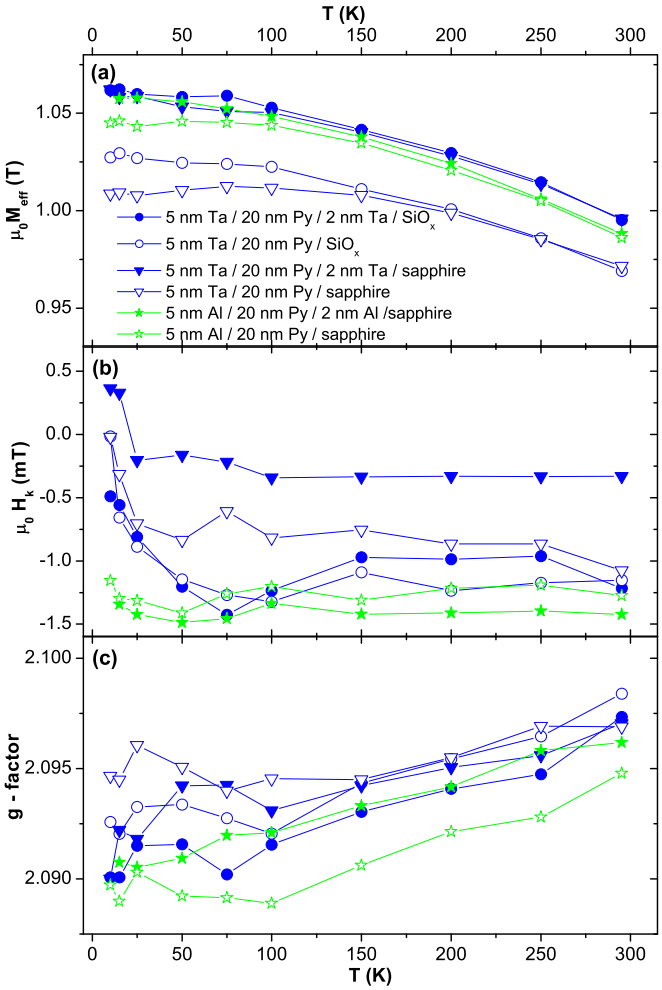

FIG. 8. Results of the Kittel fit (not shown) for the identical set of samples as in Fig. 7 summarizing the temperature-dependence of (a) M_{eff}, (b) H_{k}, and (c) the g factor. Open symbols refer to samples with cap and buffer, solid symbols to samples with cap only, respectively.

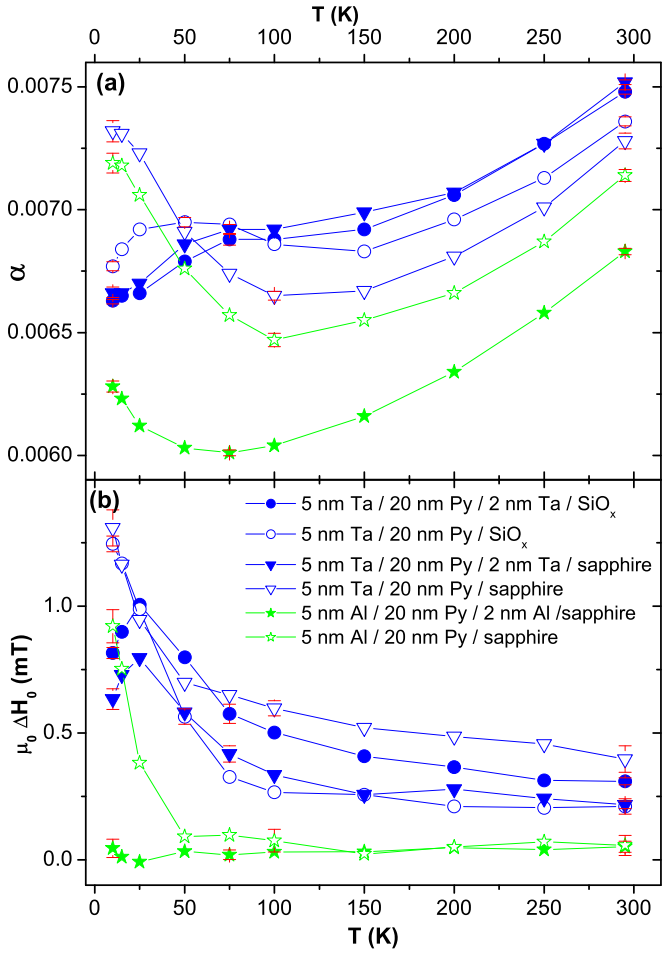

FIG. 9. Resulting Gilbert-damping parameter $\alpha(T)$ (a) and inhomogeneous broadening $\Delta H_0(T)$ (b) derived from the linear fit of the data given in Fig. 7. Solid symbols refer to samples with cap and buffer, open symbols for samples with cap only, respectively. Error bars derived from the linear regression of the data are indicated in red for selected temperatures.

Figure 8(b) summarizes the results for H_{k} for the same set of samples as in (a). Only for Ta, a very small increase of H_{k} can be seen at low temperatures, which is less pronounced for Al. This may corroborate a slightly stronger tendency for intermixing at the Ta/Py interface, which can go hand in hand with small interfacial anisotropies. The overall negative values for H_{k} were already addressed above and are most likely due to a small negative offset field of the superconducting magnet. Note that in all cases, rectangular sample pieces were cut with the long side corresponding to the in-plane easy axis, which was oriented along H_{ext}. With regard to the g factor, no significant temperature dependence is found in Fig. 8(c). All samples show identical fitted values within the visible scatter of the data. However, looking at each individual sample, a small tendency to a slight reduction of g with decreasing temperature may be inferred. For example, the Al-capped film has $g = 2.095$ at 295 K and $g = 2.090$ at low temperatures. The visible scatter in this data set is ± 0.002, so a reduction of g of about 0.1% may be inferred from this data set. This statement explicitly refers to relative changes with temperature. The accuracy of the absolute value for g in this type of experimental setup is less precise and g factors of 2.09 are at the lower end of the commonly accepted values for Py [31]. Note that such a reduction could be caused by the different thermal expansion coefficients of Py and the substrate and thus the resulting strain; however, one can consider this scenario as unlikely, since Py is known to have only weak magnetostriction, see, e.g., Ref. [26]. For the purposes of this paper, where the magnetic damping is the quantity of interest, it is important to note that within less than a percent, g is constant. Thus, it should not influence the accuracy of the extracted α since, according to Eq. (2), the value of g is needed to calculate α from the slope of the $\Delta H(f_{\mathrm{MW}})$ data.

Finally, Fig. 9 represents the central finding of the present paper, namely, the temperature dependence of α in (a), as well as the inhomogeneous broadening $\Delta H_0(T)$ in (b), which were extracted by fitting the $\Delta H(f_{\mathrm{MW}})$ data of the metal-capped (open symbols, sample type II) and sandwiched (full symbols, sample type III) Py films. A number of observations can be made: (i) Py in direct contact with a sapphire substrate (open

TABLE II. Compilation of the most important quantitative results of homogeneous and inhomogeneous magnetic damping for metallic capped and sandwiched Py films for selected temperatures as displayed in Fig. 9. The experimental error bars for α are in the range of ± 0.00002 and ± 0.00006.

	$\alpha^{300\,\mathrm{K}}$	$\alpha^{75\,\mathrm{K}}$	$\alpha^{10\,\mathrm{K}}$	$\Delta H_0^{300\,\mathrm{K}}$	$\Delta H_0^{10\,\mathrm{K}}$
Ta/Py/Ta	0.00750	0.00690	0.00664	0.3 mT	0.7 mT
Ta/Py/SiO_x	0.00736	0.00694	0.00677	0.2 mT	1.2 mT
Ta/Py/sapphire	0.00728	0.00674	0.00732	0.4 mT	1.3 mT
Al/Py/Al	0.00683	0.00601	0.00623	<0.1 mT	<0.1 mT
Al/Py/sapphire	0.00714	0.00657	0.00719	<0.1 mT	0.9 mT

triangles/stars) exhibits an increase of both α and ΔH_0 at low temperatures, whereas when in contact with a silicon substrate (open circles) only the low-temperature increase in ΔH_0 is present. (ii) Py with a Ta cap or sandwiched in Ta has a generally higher α and ΔH_0 compared to an Al cap or sandwich (blue vs green symbols). (iii) Py in direct contact to both oxidic substrates (open symbols) has a pronounced increase of ΔH_0 at low temperatures. This is partially suppressed by a Ta buffer (solid blue symbols) and is fully suppressed by an Al buffer (solid gree symbols). (iv) Py sandwiched in Ta has a higher α, especially at higher temperatures, but α decreases for low temperatures. (v) Py sandwiched in Al appears to be the best choice in terms of both low α and ΔH_0. (vi) By just focusing on the 295 K data, one can see that an Al buffer decreases α compared to an Al cap, whereas a Ta buffer increases α compared to an Ta cap. Both trends hold down to 50 K for Ta where there is a crossover. In contrast, this crossover is absent for Al and the sandwiched Py exhibits a clearly lower α for all temperatures. These observations are indicative of a more complex interplay of different effects on the FMR linewidth for the Ta/Py interface(s), e.g., Ta as a rather heavy element may exhibit significant spin pumping effects at the Ta/Al interface due to its higher spin-orbit coupling compared to Al, which may explain the overall higher magnetic damping in those films. Therefore, the Al/Py interface appears to be the most suitable choice for lowest possible homogeneous damping and close-to-zero inhomogeneous contributions.

An overview of the quantitative findings of the Py films with metallic capping and buffer layers can be found in Table II for selected temperatures. To focus on the lowest achievable damping, the Al-sandwiched Py film, the homogeneous Gilbert damping parameter α is 0.00683(2) at 295 K, it decreases to 0.00601(2) between 50 K and 100 K until it increases again to 0.00623(2) at 10 K. Thus, it is at the lower end of the various other reported values, which range from 0.004 to 0.009 as compiled in Refs. [21,22]. For a quantitative comparison of the findings in this paper, it is interesting to directly look at the respective lowest reported values in the original works: An α of 0.004 has been reported in Ref. [21], which was reported for a Ta/Py/Ta multilayer measured at a single FMR frequency [32]. Likewise, the lowest value of 0.0055 reported for TaN-capped Py in Ref. [22] was taken from Ref. [15]. It is, however, interesting to note that both values were derived from a thickness dependence of the respective Py film, and thus they represent extrapolated bulk values. If one looks at 20-nm-thick Py films, as in the present case, one finds a value for $\alpha = 0.0088(18)$ for the Ta/Py multilayer in Ref. [32] and $\alpha = 0.0064$ at 300 K for the TaN-capped Py film in Ref. [15]. Note that this value drops to about 0.0057 at 5 K; however, in those samples α exhibits a slight maximum around 50 K to 75 K, which is in contrast to the local minimum observed in the present study. Nevertheless, the homogeneous Gilbert damping parameter for Al-sandwiched Py of 20 nm thickness is among the lowest experimental values reported in the literature. Note that throughout this paper, all values have not been corrected by the radiative damping, which would further lower the intrinsinc damping, see, e.g., Ref. [22].

A final word concerns the temperature dependence of α of Al-sandwiched Py films (full green stars) in Fig. 9(a). There is a clear minimum of α around 75 K. Considering the suggested conductivity and resistivitylike contributions to the magnetic damping [16,17], this observation suggests that both contributions play a role in Py as well. The reduction in the damping parameter as the temperature is lowered to 75 K is indicative of a resistivitylike behavior, consistent with the characteristics expected for Py films [12,33]. Furthermore, the temperature-dependent trend of the damping parameter down to 75 K closely resembles the quadratic temperature dependence observed in Py resistivity [34]. The conductivitylike contribution, i.e., the low temperature increase, has recently been reported for epitaxial Fe [18], although it has been known for decades for other elemental ferromagnetic metals like Ni and Co [19]. However, in the case of Py the increase at low temperatures is much less pronounced than what is reported in the literature for elemental ferromagnets [18,19] and is consistent with the earlier findings of the absence of conductivitylike contributions for Py [33]. It should be noted that most of the older work was measured at a single frequency and, thus, homogeneous contributions were not easy to separate from inhomogeneous contributions, although the latter should be minimal for the single crystalline whiskers used in Ref. [19]. Referring to the broadband FMR studies on epitaxial Fe in Ref. [18] in comparison to the present paper on Al-sandwiched Py, further work is necessary to clarify whether the weak low-temperature increase of α for Al/Py/Al is indeed indicative of a small conductivitylike contribution to the damping in Py or if interfacial effects like those reported in Ref. [15] play an additional role.

IV. SUMMARY

In summary, we have systematically investigated a range of common capping layers and substrates to deduce a suitable material combination for the fabrication and protection of Py thin films to achieve lowest possible magnetic damping down to low temperatures. It turns out that oxide capping layers, while comparable to metallic ones at elevated temperatures, lead to a strong low-temperature increase in the FMR linewidth in terms of homogeneous and inhomogeneous contributions. In addition, two-magnon scattering processes are also evidenced. Therefore, metallic capping layers are the better choice. However, these caps should be self-passivating at ambient conditions as is the case for Ta and Al used in

this study. The second oxidic interface to the substrate is less crucial and the magnetic damping is not strongly affected for both silicon and sapphire substrates. Nonetheless, there is still a low-temperature increase of homogeneous and inhomogeneous contributions to the FMR linewidth. This can be improved by inserting a thin metallic buffer layer and Al turns out to be the better choice compared to Ta where, especially at elevated temperatures, the Gilbert-like damping is slightly increased compared to the unbuffered Py. Therefore, Al/Py/Al is found to be the most suitable choice to further investigate the fundamental magnetic properties in terms of low magnetic damping, especially at low temperatures. For example, a thickness series of Py would be of interest to disentangle interfacial from bulk contributions. In light of the present paper, a symmetric, Al-sandwiched Py would be the most promising choice of materials towards the lowest possible magnetic damping in the entire temperature range from 5 to 295 K.

[1] S. Azzawi, A. T. Hindmarch, and D. Aktinson, J. Phys. D: Appl. Phys. **50**, 473001 (2017).

[2] A. Brataas, A. D. Kent, and H. Ohno, Nat. Mater. **11**, 372 (2012).

[3] B. Divinskiy, S. Urazhdin, S. O. Demokritov, and V. E. Demidov, Nat. Commun. **10**, 5211 (2019).

[4] P. Pirro, V. I. Vasyuchka, A. A. Serga, and B. Hillebrands, Nat. Rev. Mater. **6**, 1114 (2021).

[5] H. Yu, J. Chen, V. Cros, P. Bortolotti, H. Wang, C. Guo, F. Brandl, F. Heimbach, X. Han, A. Anane, and D. Grundler, Adv. Funct. Mater. **32**, 2203466 (2022).

[6] D. Murzin, V. K. Belyaev, F. Groß, J. Gräfe, N. Perov, V. Komanicky, and V. Rodionova, J. Magn. Magn. Mater. **588**, 171398 (2023).

[7] A. Krysztofik, N. Kuznetsov, H. Qin, L. Flajsman, E. Coy, and S. van Dijken, Materials **15**, 2814 (2022).

[8] A. Barman, G. Gubbiotti, S. Ladak, A. O. Adeyeye, M. Krawczyk, J. Gräfe, C. Adelmann, S. Cotofana, A. Naeemi, V. I. Vasyuchka *et al.*, J. Phys.: Condens. Matter **33**, 413001 (2021).

[9] A. V. Chumak, P. Kabos, M. Wu, C. Abert, C. Adelmann, A. O. Adeyeye, J. Akerman, F. G. Aliev, A. Anane, A. Awad *et al.*, IEEE Trans. Magn. **58**, 1 (2022).

[10] T. L. Gilbert, IEEE Trans. Magn. **40**, 3443 (2004).

[11] L. D. Landau and E. M. Lifshitz, Phys. Z. Sowjetunion **8**, 153 (1935).

[12] B. Heinrich, Spin relaxation in magnetic metallic layers, and multilayers, in *Ultrathin Magnetic Structures III*, edited by J. A. C. Bland and B. Heinrich (Springer-Verlag, Berlin, Heidelberg, 2005), pp. 143–210.

[13] J. Lindner, K. Lenz, E. Kosubek, K. Baberschke, D. Spoddig, R. Meckenstock, J. Pelzl, Z. Frait, and D. L. Mills, Phys. Rev. B **68**, 060102(R) (2003).

[14] I. Harward, T. O'Keevan, A. Hutchison, V. Zagorodnii, and Z. Celinski, Rev. Sci. Instrum. **82**, 095115 (2011).

[15] Y. Zhao, Q. Song, S.-H. Yang, T. Su, W. Yuan, S. S. P. Parkin, J. Shi, and W. Han, Sci. Rep. **6**, 22890 (2016).

[16] R. D. McMichael and P. Krivosik, IEEE Trans. Magn. **40**, 2 (2004).

[17] K. Gilmore, M. D. Stiles, J. Seib, D. Steiauf, and M. Fähnle, Phys. Rev. B **81**, 174414 (2010).

[18] B. Khodadadi, A. Rai, A. Sapkota, A. Srivastava, B. Nepal, Y. Lim, D. A. Smith, C. Mewes, S. Budhathoki, A. J. Hauser, M. Gao, J.-F. Li, D. D. Viehland, Z. Jiang, J. J. Heremans, P. V. Balachandran, T. Mewes, and S. Emori, Phys. Rev. Lett. **124**, 157201 (2020).

[19] S. M. Bhagat and P. Lubitz, Phys. Rev. B **10**, 179 (1974).

[20] B. Heinrich, D. J. Meredith, and J. F. Cochrane, J. Appl. Phys. **50**, 7726 (1979).

[21] A. A. Starikov, P. J. Kelly, A. Brataas, Y. Tserkovnyak, and G. E. W. Bauer, Phys. Rev. Lett. **105**, 236601 (2010).

[22] M. A. W. Schoen, J. Lucassen, H. T. Nembach, B. Koopmans, T. J. Silva, C. H. Back, and J. M. Shaw, Phys. Rev. B **95**, 134411 (2017).

[23] C. Gonzalez-Fuentes, R. K. Dumas, and C. Garcia, J. Appl. Phys. **123**, 023901 (2018).

[24] M. Buchner, K. Lenz, V. Ney, J. Lindner, and A. Ney, New J. Phys. **25**, 073002 (2023).

[25] D. J. Twisselmann and R. D. McMichael, J. Appl. Phys. **93**, 6903 (2003).

[26] M. Salou, B. Lescop, S. Rioual, A. Lebon, J. Ben Youssef, and B. Rouvellou, Surf. Sci. **602**, 2901 (2008).

[27] S. Lecuyer, A. Quemerais, and J. Jezequel, Surf. Interface Anal. **18**, 257 (1992).

[28] M. Kowalewski, W. H. Butler, N. Moghadam, G. M. Stocks, T. C. Schulthess, K. J. Song, J. R. Thompson, A. S. Arrott, T. Zhu, J. Drewes, R. R. Katti, M. T. McClure, and O. Escorcia, J. Appl Phys. **87**, 5732 (2000).

[29] G. H. Yu, H. C. Zhao, M. H. Li, F. W. Zhu, and W. Y. Lai, Appl. Phys. Lett. **80**, 455 (2002).

[30] D. Marko, T. Strache, K. Lenz, J. Fassbender, and R. Kaltofen, Appl. Phys. Lett. **96**, 022503 (2010).

[31] J. M. Shaw, H. T. Nembach, T. J. Silva, and C. T. Boone, J. Appl. Phys. **114**, 243906 (2013).

[32] J. O. Rantschler, B. B. Maranville, J. J. Mallett, P. Chen, R. D. McMichael, and W. F. Egelhoff Jr., IEEE Trans. Magn. **41**, 3523 (2005).

[33] S. Ingvarsson, L. Ritchie, X. Y. Liu, G. Xiao, J. C. Slonczewski, P. L. Trouilloud, and R. H. Koch, Phys. Rev. B **66**, 214416 (2002).

[34] G. Counil, T. Devolder, J.-V. Kim, P. Crozat, C. Chappert, S. Zoll, and R. Fournel, IEEE Trans. Magn. **42**, 3323 (2006).